

**Characterization of Ultrashort Optical Pulses by
Spectral Shearing Interferometry**

Jay Amin

Rush-Henrietta Senior High School
Henrietta, NY

Advisor: Dr. Christophe Dorrer

Laboratory for Laser Energetics
University of Rochester
Rochester, NY

Summer 2008

Abstract

Ultrashort optical pulses are integral to various fields. Thus, the characterization of these pulses is crucial in understanding the results of experiments and applications using them. A diagnostic for laser systems was created to determine the shapes of ultrashort optical pulses using the principle of spectral shearing interferometry (SSI). By strongly chirping an optical pulse using a pair of parallel diffraction gratings and mixing it in a lithium triborate LiB_3O_5 (LBO) nonlinear crystal with two test pulse replicas delayed by 1.9 ps, sum harmonic generation of the input laser beam was achieved. The SSI interferogram was then characterized by an Ocean Optics Spectrometer using a novel “ 2ω method” to determine pulse characteristics. The diagnostic was tested on the diagnostic compressor of the Multi-TeraWatt (MTW) laser system at the Laboratory for Laser Energetics, successfully determining the compressor distance for which the optical pulses were shortest.

1. Introduction

Ultrashort optical pulses are widely used in several areas of physics. Common usages are in high-speed optical communications and high-temporal-resolution spectroscopy of physical systems. In optical telecommunications, using the shortest optical pulses possible allows for the greatest amount of data to be sent in a given period. Other usages include high-intensity laser-matter interactions. Using chirped pulse amplification, a short optical pulse can be stretched, amplified, and compressed, producing a final short pulse with very high power.^{1,2} Experimental usages of ultrashort optical pulses cannot be deemed accurate unless the shape of the test pulses is as

intended. Thus knowing the temporal shape of optical pulses is crucial to scientific research.

The most significant obstacle to determining the shapes of pulses is that direct measurements in the time domain using a photodetector are simply not fast enough, for ultrashort pulses are on the order of femtoseconds. Therefore, measurements must be made in the spectral domain and the temporal shape of the pulse must be calculated from the data using a Fourier transform. There are currently three categories of methods used to accurately determine the shapes of these pulses, fundamental to physical theories: spectrographic, tomographic, and interferometric.^{3,4} The spectrographic methods are most commonly used, with frequency-resolved optical gating (FROG)⁵, frequency-domain phase measurements (FDPM)⁶, and the spectrally and temporally resolved upconversion technique (STRUT)⁷ among the many that require sophisticated data inversion techniques and algorithms to reconstruct the electric field. Tomography, though having a noniterative data inversion method⁸, requires the one-dimensional field to be represented in two dimensions, thus increasing greatly the amount of data that must be collected. Interferometric techniques, therefore, are the simplest direct method that can be used to characterize optical pulses using properties such as electric field and phase, for they only need a one-dimensional data set to model the one-dimensional field, and can utilize a simple direct data inversion to determine pulse characteristics. The novel, self-referencing interferometric technique used by Iaconis and Walmsley⁹, referred to as spectral phase interferometry for direct electric-field reconstruction (SPIDER), is employed in this study. This method is particularly popular for its collinear geometry, its

lack of moving parts, and its lack of reliance on a fast detector or a well-characterized reference pulse.⁹

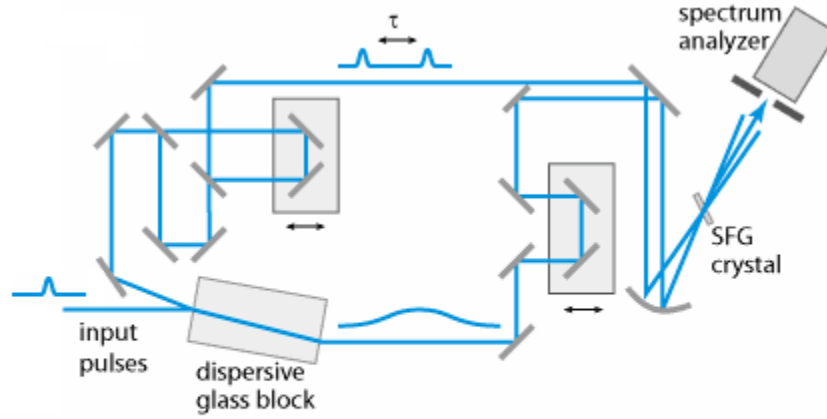


Figure 1. A setup for ultrashort optical pulse characterization using the SPIDER method.

As shown in Fig. 1, the key to the SPIDER method is splitting the test pulse in two, so that one pulse can be split into two identical copies separated by a time delay using a Michelson interferometer, for example, and the other can be stretched with a dispersive block, for example. Stretching a pulse chirps it so that its frequency varies linearly with time. Spectral shearing occurs when the chirped pulse and the two identical copies of the test pulse are mixed in a sum-frequency generating (SFG) crystal. The spectral shear refers to the difference in optical frequencies represented by the two identical copies when overlapped on the chirped pulse after upconversion. This process was utilized, in concept, for the diagnostic created and described in this paper. However, key changes were made that allow the device to be more stable, simple, and cost effective. These changes include replacing the Michelson interferometer with an etalon, using a grating pair to stretch the pulse rather than a dispersive glass block, and

converging the two focused pulse beams with a planoconvex lens instead of a convex mirror.

2. Spectral Shearing Interferometry

Since photodetectors were too slow to make direct measurements of ultrashort optical pulses, spectral shearing interferometry (SSI) based diagnostics were created so that we could indirectly make measurements of the ultrafast pulses using these photodetectors. A commonly-used spectral shearing interferometer is shown in Fig. 2.³ The interferometer creates two replicas of the test pulse using a beamsplitter. One beam is delayed by a linear spectral phase modulator and the other is frequency shifted by a linear temporal phase modulator. Then, the two pulses are recombined on another beamsplitter, allowing the resulting signal to be resolved using a spectrometer.

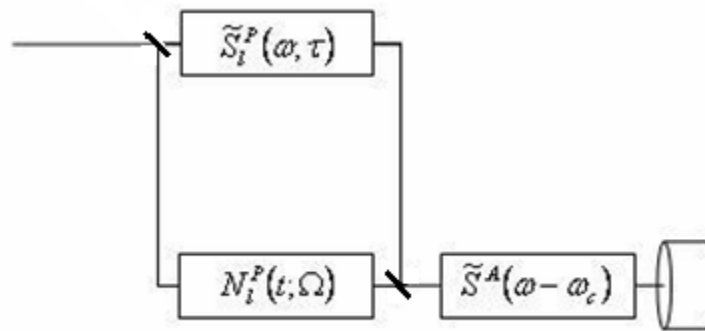


Figure 2. An SSI-based interferometer with two parallel phase filters.

The temporal phase modulator shifts the spectrum of the input pulse by Ω , noted in the figure by its response function

$$N_i^P(t; \Omega) = \exp[-i\Omega t] \quad (1)$$

where N is the nonstationary filter, P indicates that it is a phase-only filter, and l means the phase modulation is linear. Similarly, the linear spectral phase modulator has a response function of

$$\tilde{S}^P_l(\omega; \tau) = \exp[i\omega\tau] \quad (2)$$

which states that the input pulse is delayed by τ . The signal after the two pulses are combined and passed through a spectrometer is

$$D(\omega_c; \Omega, \tau) = \int d\omega |\tilde{S}^A(\omega - \omega_0) \cdot \{[\int d\omega' \tilde{N}^P_l(\omega' - \omega_0) \tilde{E}(\omega')] + \tilde{S}^P_l(\omega) \tilde{E}(\omega)\}|^2 \quad (3)$$

where the electric fields of the optical pulses are recorded as a function of the filter parameters for N and the Fourier transform of the pulse's output energy, $\tilde{E}(\omega)$, is

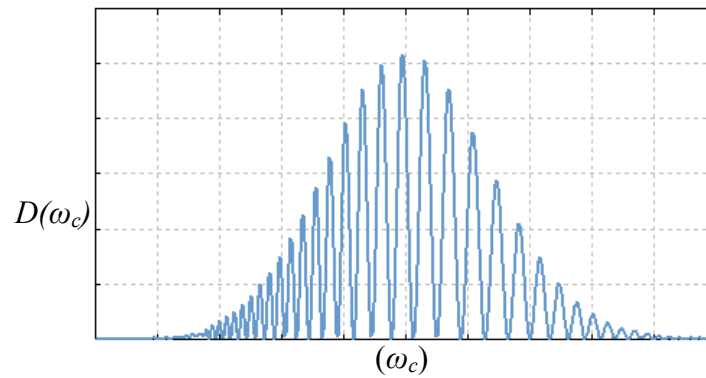


Figure 3. A general spectral interferogram of the interference between two spectrally sheared pulses.

recorded as a function of the filter parameters for S . Thus, it is also multiplied by the amplitude-only time-stationary filter of the spectrometer, \tilde{S}^A , which was used to resolve the signal. Since the spectral shift and temporal delay are fixed, the signal can be re-expressed as

$$D(\omega_c) = |\tilde{E}(\omega_c - \Omega)|^2 + |\tilde{E}(\omega_c)|^2 + 2|\tilde{E}(\omega_c - \Omega) \tilde{E}(\omega_c)| \cos[\Phi_\omega(\omega_c - \Omega) - \Phi_\omega(\omega_c) - \tau\omega_c]. \quad (4)$$

where $D(\omega_c)$ is a standard shearing interferogram as shown in Fig. 3.

3. Determining the Spectral Phase

The spectral phase of the data can be obtained from the interferogram by analyzing the relative positions of the fringes which are nominally spaced in frequency by $2\pi/\tau$ as shown in Fig. 3. This is done by rewriting the interferogram as

$$D(\omega_c) = D^{(dc)}(\omega_c) + \exp[-i\tau\omega_c]D^{(-ac)}(\omega_c) + \exp[i\tau\omega_c]D^{(+ac)}(\omega_c). \quad (5)$$

where

$$D^{(dc)}(\omega_c) = |\tilde{E}(\omega_c - \Omega)|^2 + |\tilde{E}(\omega_c)|^2. \quad (6)$$

$$D^{(-ac)}(\omega_c) = |\tilde{E}(\omega_c - \Omega) \tilde{E}(\omega_c)| \exp[i(\Phi_\omega(\omega_c - \Omega) - \Phi_\omega(\omega_c))]. \quad (7)$$

and thus

$$D^{(+ac)}(\omega_c) = |\tilde{E}(\omega_c - \Omega) \tilde{E}(\omega_c)| \exp[-i(\Phi_\omega(\omega_c - \Omega) - \Phi_\omega(\omega_c))]. \quad (8)$$

This rewritten interferogram is Fourier transformed as first shown by Takeda, et al.¹⁰

$$\begin{aligned} \tilde{D}(t) = & FT\{D^{(dc)}(\omega_c); \omega_c \rightarrow t\} \\ & + FT\{D^{(-ac)}(\omega_c); \omega_c \rightarrow t + \tau\} \\ & + FT\{D^{(+ac)}(\omega_c); \omega_c \rightarrow t - \tau\}. \end{aligned} \quad (9)$$

Fig. 4 shows the Fourier transform of the interferogram. The dc term centered at $t=0$ is the sum of the two spectra for the pulses, and since having no phase information, this is filtered away. The ac term at $-\tau$ is also filtered away because only one ac term,

that at $t=\tau$, is needed to generate the spectral phase. This is accomplished with a fourth-order super-Gaussian filter, $H(t)$, of full width τ and centered at $t=\tau$:

$$\tilde{D}^{(filter)}(t) = H(t - \tau) \tilde{D}(t) = FT\{D^{(+ac)}(\omega_c); \omega_c \rightarrow t - \tau\}. \quad (10)$$

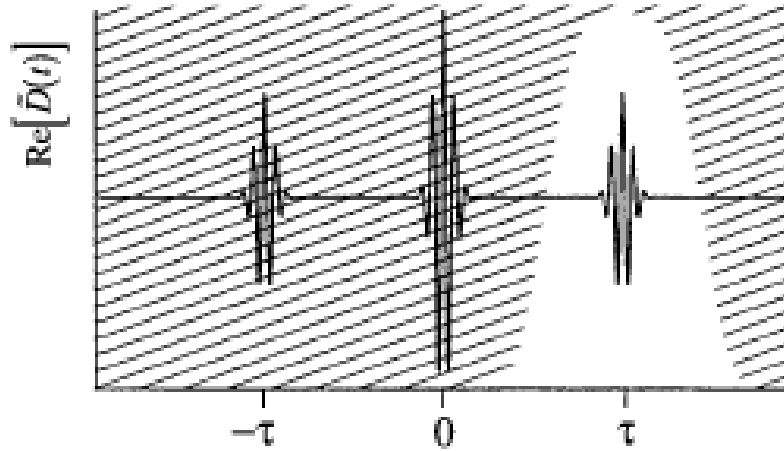


Figure 4. The Fourier transform of the interferogram in Fig. 3. The shaded region represents the section of the function that is ignored by the filter.

The desired spectral phase difference is simply the argument of the inverse transform of $\tilde{D}^{(filter)}(t)$, which is also the isolated ac term is:

$$\Phi_{\omega}(\omega_c) - \Phi_{\omega}(\omega_c - \Omega) + \tau\omega_c = \arg [D^{(+ac)}(\omega_c)] = \arg [IFT\{\tilde{D}^{(filter)}(t); t \rightarrow \omega_c\}]. \quad (11)$$

Then the linear phase term $\tau\omega_c$ must be removed by subtracting a baseline linear phase. This baseline linear phase is determined by using an interferometer to record the spectral interferogram of the pair of pulses without the spectral shear. Finally, the spectral phase can be reconstructed from the spectral phase difference by concatenation.

Concatenation returns the spectral phase at intervals of Ω across the spectrum, so the spectral phase at some frequency is set equal to zero allowing the spectral phase for all frequencies to be multiples of the spectral shear away from ω_0 . By adding all the

phase differences, the phase for frequencies separated by the spectral shear is reconstructed.

4. Methodology

The diagnostic which was built utilizes the SSI method of SPIDER with the previously mentioned novel innovations. The key elements in these innovations, outlined in Fig. 5, will be discussed in this section.

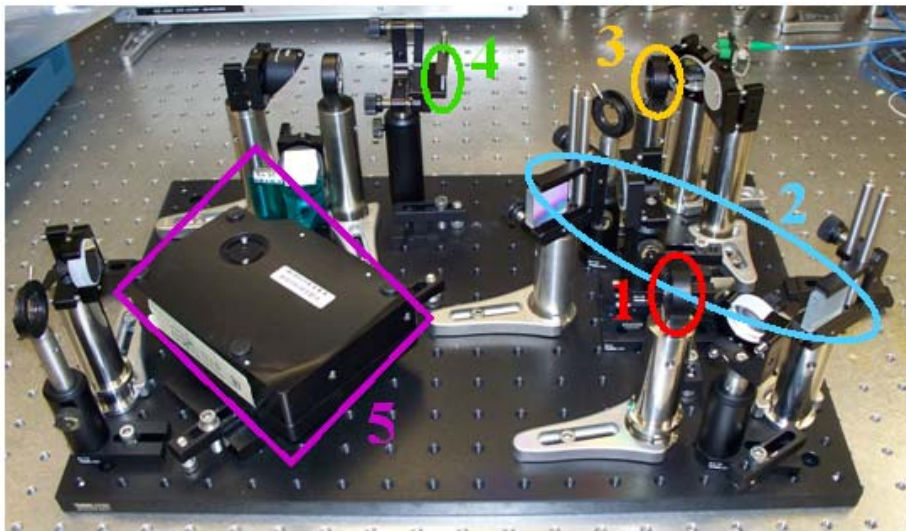


Figure 5. The SSI diagnostic built for this study. Labeled are the key elements of the diagnostic. (1) Etalon (2) Double-pass two-grating compressor (3) Planoconvex Lens (4) Nonlinear crystal (5) Ocean Optics Spectrometer.

4.1 Generation of Time-Delayed Replicas Using an Etalon

There are two limitations to the value that can be used for the relative delay between pulses in the test pair. The delay, τ , must not be so large that the spectrometer cannot resolve the fringes in the interferogram, but not so small that the data inversion

routine cannot separate the *dc* and *ac* terms. Therefore, to generate the time-delayed replicas, there are two main approaches: the usage of an interferometer, such as the

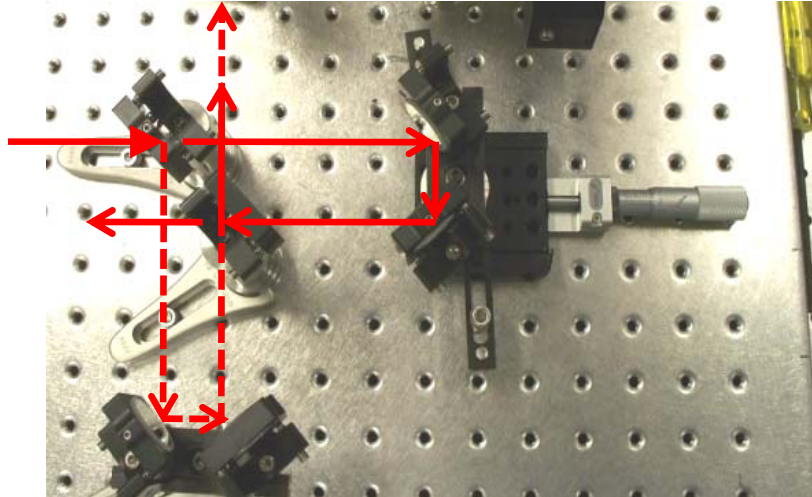


Figure 6. A Michelson interferometer built during this internship for another project. Solid red arrows indicate transmitted beams through the beamsplitters and the dashed arrows represent reflected beams.

Michelson; or an etalon. The Michelson interferometer (Fig. 6) utilizes two gold-plated beamsplitters: one to divide the incoming test pulse into two arms, one of which has a variable distance due to the mounting of a set of perpendicular mirrors on a translation stage, and the other to recombine the pulses from the two arms. On the other hand, the etalon is a simple glass microscope slide that reflects $\sim 4\%$ of the incoming light on each of its two faces, separated by 0.20 mm. This delays the reflections from each face in this diagnostic by nearly 1.9 picoseconds. Interferometric accuracy requires stability in τ since jitter between the test pulses can destroy phase information. An etalon is unaffected by such vibrations, while a Michelson requires additional stabilization. The etalon is more stable, compact, and less expensive than a Michelson interferometer,

which must be carefully aligned and checked before every test due to its numerous components. Therefore, an etalon was used.

4.2 Generation of the Chirped Pulse

The etalon allows ~92% of the incoming light to transmit directly through into what is called the double-pass two-grating compressor. By arranging two diffraction gratings parallel to each other so that the diffracted beam of one grating diffracts off the other, ultrashort pulses are stretched and chirped.¹¹ The diffraction of the input test pulse in the compressor effectively chirps the pulse. This means that the different frequencies of the light are separated so that they arrive in a staggered fashion with respect to one another. The gratings in the device created are ruled with 1200 lines/mm and the second order dispersion of the chirped pulse caused by these gratings shifts the phase by a stretcher dispersion of $\Phi'' = -1.3 \text{ ps}^2$. Therefore, since $\Omega = -\tau / \Phi''$, Ω , the spectral

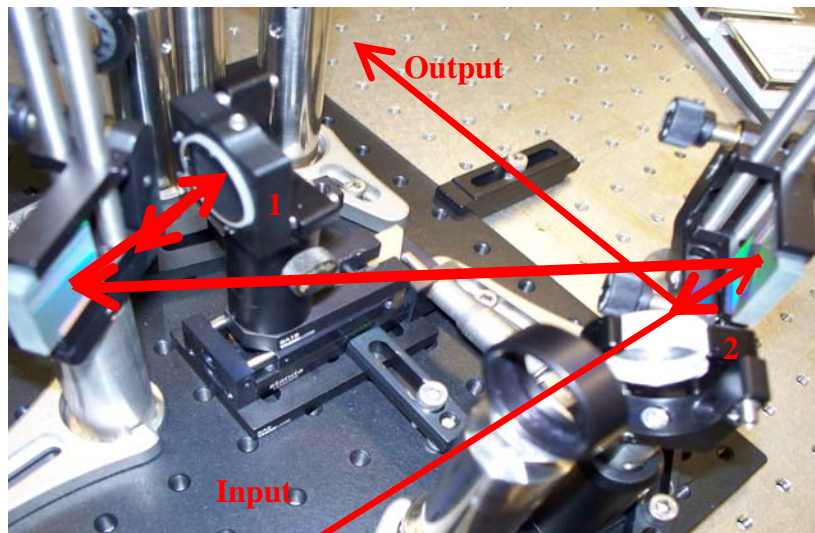


Figure 7. The input pulse travels along the same path as it exits but at a different angle, due to the tilting of mirror #1 (on the left). This allows the beam to reflect off mirror #2 in the bottom right corner, sending the chirped pulse to the output of the compressor.

separation of the two replicas in the pulses reflected off the etalon after nonlinear conversion with the chirped pulse will be 1.45 ps^{-1} , which is roughly a wavelength separation of 0.8 nm. A particularly useful feature of the double-pass two-grating compressor created in the diagnostic was the mounting of a mirror on a translation stage (mirror #1 on Fig. 7), perpendicular to the beam diffracted by the second diffraction grating. This ensured that the beam was collimated when entering the compressor on the second pass and allowed the compressor distance to be changed so that the chirped pulse and the sheared replicas would temporally overlap in the nonlinear crystal used for sum harmonic generation.

4.3 Sum Harmonic Generation in a Nonlinear Crystal

Before the two replicas of the test pulse and the chirped pulse beam can be mixed in the nonlinear crystal they must be focused. A planoconvex lens with a focal length of 15 cm was used to focus the two parallel input beams, causing them to intersect in the crystal (Fig. 8). This is particularly significant because when the beam from the

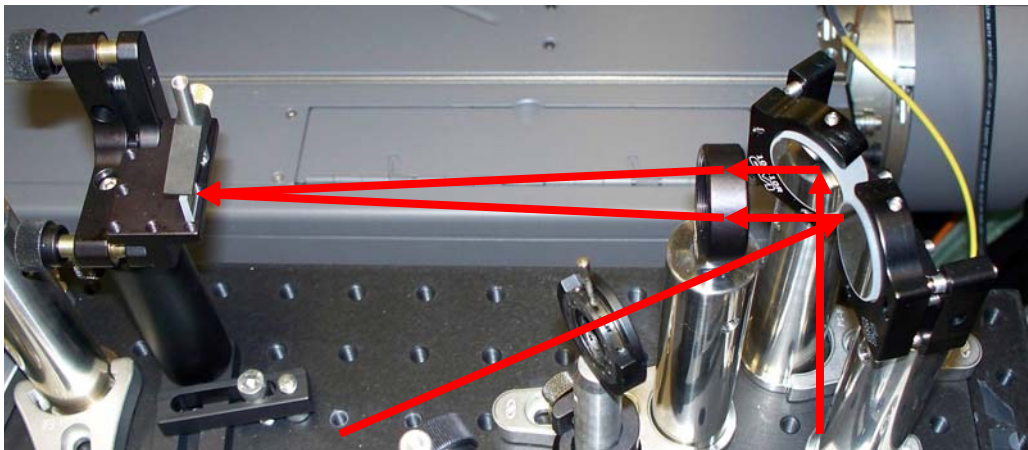


Figure 8. The alignment mirrors on the right redirect the chirped pulse beam and the replicated pulse beam, making them parallel as they enter the planoconvex lens. The lens focuses the two beams so that they intersect in the nonlinear crystal.

compressor is overlapped with the beam reflected from the etalon, each of the replicas in the reflected beam off the etalon should match up with a distinct frequency on the chirped pulse. Thus, the pulses can be separated temporally by τ and also separated spectrally by Ω . To mix the two signals into one that can be resolved by a spectrometer, they are nonlinearly converted. Though often generalized as sum frequency generation, second harmonic generation (SHG) doubles the frequency of the input light source, thus halving the wavelength. Therefore, the Nd:YLF laser source used that operated at 1053 nm was effectively converted to 526.5 nm as the frequency changed from ω to 2ω , converting the input beam of infrared light to green light. An interferogram in the green is therefore read by the spectrometer.

The crystal used was a 2 mm biaxial LBO, LiB_3O_5 , which was cut for SHG phase-matching at 11.8° . The Type I SHG caused by this crystal guarantees that the ordinary polarized inputs of the chirped pulse and the sheared pulses will create a pulse of twice the original frequency. Both the chirped pulse and sheared pulse beam polarizations were aligned with the ordinary axes of the crystal. The beams were carefully overlapped in the crystal temporally by adjusting the path lengths of the reflected and transmitted beams from the etalon, and spatially, using the alignment mirrors. By carefully adjusting the x- and y-orientation angles of the crystal, SHG was optimized to yield a measurable signal.

4.4 Resolving the Spectral Interferogram

A CCD array at the output of a spectrometer can resolve the spectral interferogram, once properly calibrated. The spectrometer used, an Ocean Optics HR2000, has a resolution of 0.5 nm at 1053 nm. Thus it could effectively resolve the

fringes separated by $2\pi/\tau$, a delay of 1.9 ps. Fig. 9 is a sample SSI interferogram of the upconverted pulses after passing through the diagnostic.

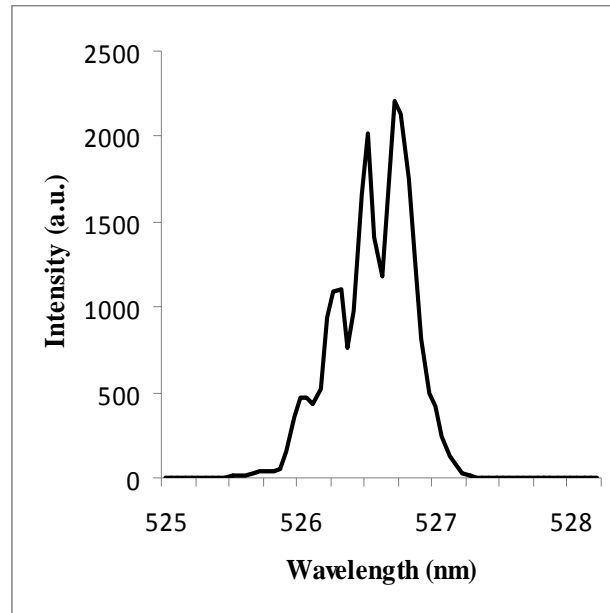


Figure 9. The SSI interferogram from the diagnostic. The ideal Gaussian shape of the pulse is not clearly apparent due to the low resolution of the spectrometer on this scale, which shows fringe points. However, the pulse is shown to have been effectively upconverted due to the centering on $\lambda_{input}/2$, which is 526.5 nm.

The technique created and employed in the capturing of the interferogram was aptly dubbed the “ 2ω method.” Spectrometers contain a diffraction grating that allows the input pulse to have all of its frequencies separated, similar to the chirping of the double-pass two-grating compressor in the diagnostic (see Fig. 10). The properties of the diffraction grating can be summarized by the equation

$$\sin(\theta_i) + \sin(\theta_d) = n\lambda / d \quad (12)$$

where θ_i is the incidence angle on the grating, θ_d is the diffracted angle off the grating, n is the order of diffraction, λ is the wavelength of the input light, and d is the groove

spacing of the diffraction grating. The unique aspect of this simple equation in the operation of the diagnostic is that both the SSI interferogram following nonlinear

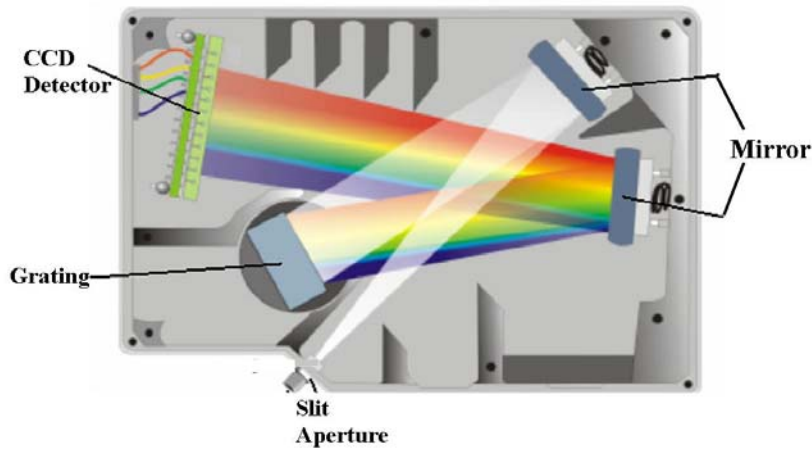


Figure 10. The schematic for the Ocean Optics HR2000 spectrometer.

conversion and the spectrum of the pulse under test can be determined by the spectrometer without additional calibration. The quantities d and $\sin(\theta_i)$ are constant because d is a property of the grating and the incidence angle on the grating will not change if the properties of the light source are changed. At ω , the λ of the input light is 1053 nm and first-order diffraction occurs. However, at 2ω , λ is 526.5 nm; therefore, second-order diffraction occurs. Thus, both types of light cause the same diffracted angle and can be read directly by the spectrometer. Each CCD pixel corresponds to a certain frequency of light, so even if every frequency in the light pulse is doubled, the pulse shape of the output will still be the same when determined by the spectrometer.

5. Results

The diagnostic was tested on the Multi-Terawatt (MTW) laser system, a 5 Hz, optical parametric chirped-pulse amplifier laser system, capable of delivering >250 mJ of energy per pulse.

The diagnostic compressor of MTW is similar to the grating pair in the diagnostic in that there are two diffraction gratings parallel to each other (Fig. 11); however, the diagnostic compressor of MTW is used to create ultrashort pulses, rather than chirp them. The diagnostic was set at the output of the diagnostic compressor chamber to measure these pulses. By altering, lengthwise, the position of diffraction grating #2 (on the right in Fig. 11), the ultrashort pulses being sent through the laser system were stretched and

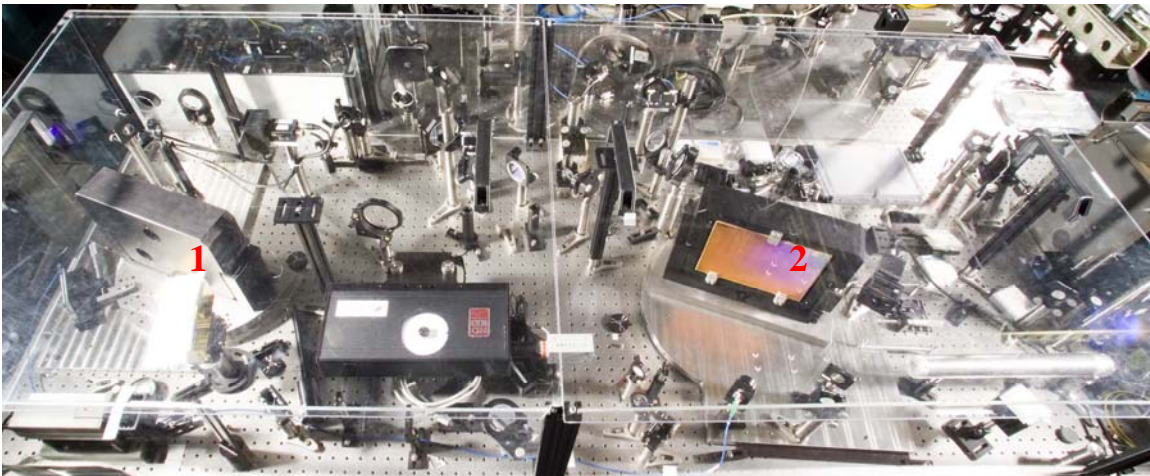


Figure 11. The diagnostic compressor of MTW. The diffraction gratings are labeled 1 and 2. Grating #2 was adjusted longitudinally to determine the best compressor distance for creating ideal ultrashort optical pulses.

compressed. The diagnostic was able to determine the distance that would induce the most linear phase over the given temporal domain, which would in turn create the ideal ultrashort, Gaussian optical pulse. A reference distance between the gratings was already known for creating the shortest pulses and the diagnostic was able to accurately confirm this distance, noted as “Reference” in Fig. 12a, b.

The diagnostic was successful in confirming that the reference distance between

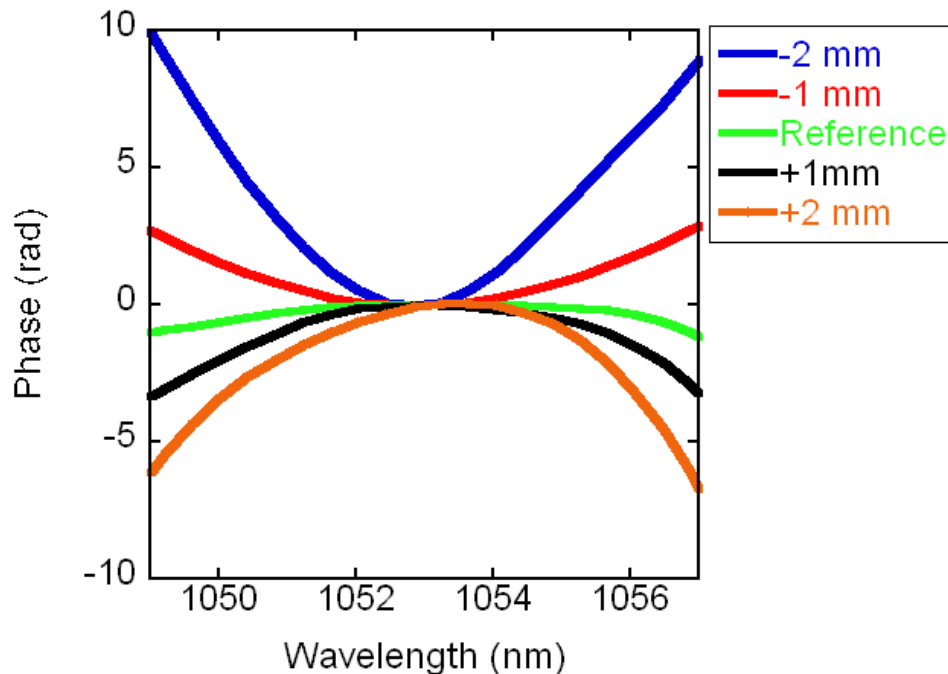


Figure 12a. The spectral phases of the ultrashort pulses created by changing the distance of the diagnostic compressor in MTW. The reference distance has the most linear phase, indicating that the temporal shape of the pulse will be most ideal.

the gratings in the diagnostic compressor was the ideal distance for creating the shortest pulses. As Fig. 12a shows, the spectral phase of the measured pulse at the Reference distance is most linear over the domain of the pulse's spectrum. The greater the difference in distance between the gratings from Reference, the more quadratic the phases became, indicating that the temporal shapes of these pulses had been stretched and their durations increased. The temporal shapes of the pulses were then determined in essence by Fourier transforming the spectral representation of the pulse (i.e. determined from the measured optical spectrum and spectral phase). The diagnostic confirms the predictions from the phases. By changing the longitudinal distance between the two diffraction gratings by ± 1 mm from Reference, the shape of the pulse was effectively stretched from 450 ± 5 femtoseconds to 1.7 ± 0.01 picoseconds, measured as full width at half maximum (FWHM), confirming the shapes of the phases and the accuracy of the

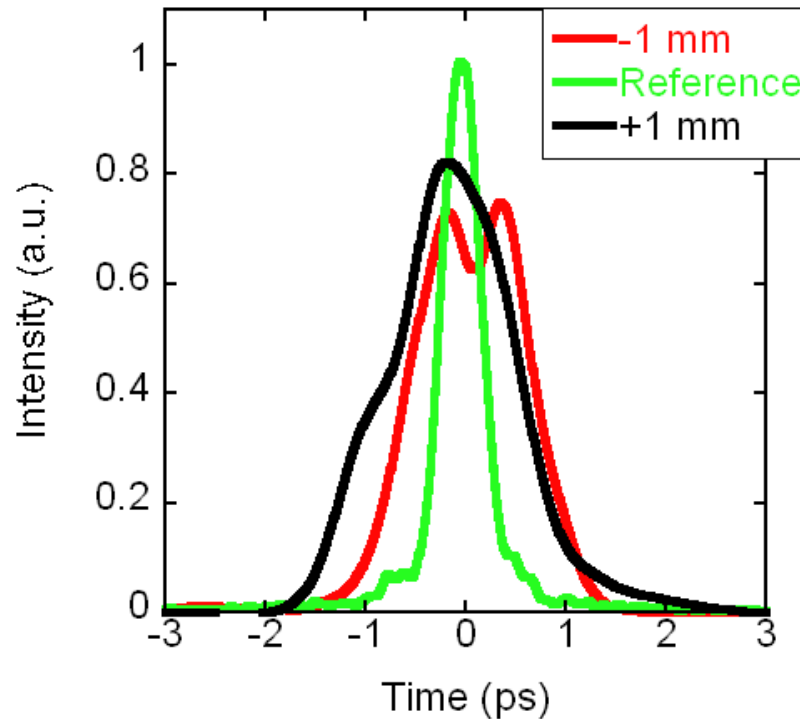


Figure 12b. The SSI interferogram of the pulses from the diagnostic compressor of MTW. The “Reference” distance is clearly the ideal distance for the grating compressor. Changes of ± 1 mm greatly altered the shape of the ultrashort Gaussian pulse by temporally stretching its shape.

diagnostic (Fig. 12b). Future experiments have been planned to determine the accuracy of the diagnostic further.

6. Discussion

The diagnostic was able to accurately perform as planned using the concept of spectral shearing interferometry. The temporal shapes of ultrashort optical pulses were determined by characterizing the spectral properties of phase and intensity. These characteristics were determined in a simple, reliable, and noniterative fashion that only required the use of two Fourier transforms and no complex algorithms. Overall, the

method required less data than either tomographic or spectrographic techniques and can be easily adapted to ultraviolet light sources by downconversion, as well as infrared by upconversion. The diagnostic is self-referencing and has no moving parts and is entirely collinear, allowing greater stability and thus, greater reliability. Relatively thick nonlinear crystals can be used in this diagnostic as long as the phase can be reconstructed using the spectral fringes and once properly aligned, the spectrometer and nonlinear interaction do not need to be recalibrated.

This diagnostic will be used to characterize ultrashort optical pulses on various laser systems at the Laboratory for Laser Energetics. The abilities of the diagnostic range from general characterization of pulses by determining spectral phase to confirming the effectiveness of chirped pulse amplification and compression.

7. Acknowledgments

I would like to thank my advisor Dr. Christophe Dorrer for his inspirational guidance and support during the project and the building of the diagnostic. I would also like to thank Dr. R. S. Craxton and the University of Rochester's Laboratory for Laser Energetics for allowing me to be part of the scientific research community.

8. References

1. D. Strickland and G. Mourou, *Opt. Commun.* 56, 219 (1985).
2. N. Ross, P. Matousek, M. Towrie, A. J. Langley, and J. L. Collier, *Opt. Commun.* 144, 125 (1997).
3. I. A. Walmsley and V. Wong, *J. Opt. Soc. Am. B* 13, 2453 (1996).

4. C. Iaconis, V. Wong, and I. A. Walmsley, *IEEE J. Select. Topics Quantum Electron.*, 4, 285 (1998).
5. D. J. Kane and R. Trebino, *IEEE J. Quantum Electron.*, 29, 571 (1993).
6. V. Wong and I. A. Walmsley, *J. Opt. Soc. Amer. B*, 14, 944 (1997).
7. J. L. A. Chilla and O. E. Martinez, *Opt. Lett.*, 16, 39 (1991).
8. H. R. Lange, M. A. France, J. F. Ropoche, B. S. Prade, P. Rousseau, and A. Mysyrowicz, *J. Select. Topics Quantum Electron.*, 4, 295 (1998).
9. C. Iaconis and I. A. Walmsley, *Opt. Lett.*, 23, 792 (1998).
10. M. Takeda, H. Ina, and S. Kobayashi, *J. Opt. Soc. Amer.*, 72, 156 (1982).
11. E. B. Treacy, *IEEE J. Quantum Electron.*, 5, 454 (1969).